JOURNAL OF Applied Polymer SCIENCE

Infrared spectral analysis of low concentration magnetoactive polymers

Nina Prem, Dirk Sindersberger, Gareth J. Monkman
Mechatronics Research Unit, OTH-Regensburg, Germany
Correspondence to: N. Prem (E-mail: nina.prem@oth-regensburg.de)

ABSTRACT: This work concerns an area of magnetoactive polymer (MAP) research seldom considered. Traditionally only MAP with high concentrations of magnetic filler (typically between 10 and 90 wt%) have been investigated. This article deals with a hitherto neglected aspect of research, namely MAP containing lower magnetic filler concentrations (1 to 3 wt%). This article utilizes a range of spectroscopic analysis methods (Raman and FTIR) and their applicability to MAP characterization at wavelengths ranging from 2.5 to 25 μm. Particular attention is paid to low carbonyl iron particle (CIP) concentrations in MAP for which the emergence of capillary doublets at a critical 2 wt% concentration is revealed. This results in measurable magnetic field-dependent changes in IR absorption at a wavelength of 4.255 μm together with a detectable CO_2 susceptibility. © 2019 The Authors. *Journal of Applied Polymer Science* published by Wiley Periodicals Inc. J. Appl. Polym. Sci. **2020**, *137*, 48366.

KEYWORDS: magnetism and magnetic properties; sensors and actuators; spectroscopy

Received 12 March 2019; accepted 21 July 2019
DOI: 10.1002/app.48366

INTRODUCTION

Hitherto MAP research has concentrated on compounds containing high CIP concentrations. Applications vary from magneto-mechanical control [1,2] to the immobilization of cells and enzymes.[3,4]

Consideration of the high-frequency dielectric properties of MAP is important in the design of modern sensory elements associated with applications such as soft robotics. The majority of current research concentrates on lower frequency ranges[5] with a few investigations at microwave levels.[6]

A number of optical properties on the surface of MAP have previously been investigated,[7,8] and X-Ray scattering has also been intensively researched elsewhere.[9] Consequently, spectroscopy at wavelengths shorter than 1 μm are not considered here. However, X-ray tomography is included within this study as an investigative tool in explaining many of the resulting IR spectroscopic findings.

MAP has occasionally been the subject of spectroscopic analysis, usually on a secondary basis in order to verify other findings.[10,11] The more usual MAP compounds containing higher ferromagnetic or paramagnetic content (40‐80 wt%) have previously been subjected to FTIR spectral investigation but without decisive results with regard to the influence of an applied magnetic field.[2,12]

MAP with high CIP concentration can be obtained from the Russian State Scientific Research Institute of Chemistry and Technology of Organoelement Compounds (GNIIChTEOS), but there is nothing commercially available in low concentration MAP. It must also be pointed out, that high CIP concentrations in MAP tend to form local aggregates with different properties to the rest of the bulk. Little, if anything has been carried out with lower weight percentages of CIP. This work concentrates on compounds containing less than 3 wt% ferrous particulate content.

This research deals with the behavior of low CIP concentration MAPs within the infrared spectrum (wavelengths ranging from 2.5 to 25 μm). Various MAP samples, with and without the influence of an externally applied magnetic field, are the subject of both transmission and reflection spectral analysis. Using Fourier transform infrared (FTIR) methods, the transmission of infrared radiation through MAP samples was analyzed whereas Raman techniques were used for MAP surface analysis through reflection of radiation. All measurements have been carried out at ambient temperature and pressure.

Infrared spectroscopy is generally a structure/material analysis tool whose function is based on the interaction between electromagnetic radiation in the IR wavelength range and the molecular structure of a sample. The atoms within the molecules absorb vibrational and rotational energy. A transmission spectrum is thus obtained by passing radiation through a sample and then detecting the amount of incoming radiation transmitted at a given wavelength. The energy absorbed or transmitted corresponds to the characteristic vibration of a particular chemical bond in a molecule.

Similar to infrared spectroscopy, Raman spectroscopy is a vibrational spectroscopic analysis technique and is often applied as a supplementary method. Since Raman spectroscopy is based on the reflection of radiation, only the surface of a sample is analyzed.

SAMPLE FABRICATION AND PREPARATION

The polymer used in this work is an addition-curing RTV-2 silicone (SF00, Silikonfabrik). The mechanical and electrical properties of silicones, and particularly poly(dimethylsiloxane)[13] and their behavior in the infrared range/spectrum[14] are well known. Curing is achieved by mixing two components A (base) and B (catalyst with platinum complex), proportionately 1:1, as illustrated in Figure 1. A different ratio of A or B generally leads to an incomplete curing.

The crosslinking process takes place at temperatures above 10 °C, in this case at room temperature (22 °C) and may be accelerated using higher temperatures up to 200 °C, see Table I. The pH value is almost 7 and contrary to condensation-curing silicones plays a subordinate role in the crosslinking process of addition-curing MAPs.

The carbonyl iron particles used (CIP SQ from BASF) are both mechanically and magnetically soft with diameters between 3.9 and 5 µm. CIP SQ has a pure iron (Fe) content of up to 99,8%. This differs considerably from MAP containing nano-particles or micro-particles in solution where ionic strength must be considered.[16] In traditional MAPs, the CIP are embedded in a PDMS matrix and make up between 10 and 90 wt% of the mass of the entire mixture.[1] In this work, a much lower CIP concentration is employed, and the PDMS matrix is relatively soft (Shore A00 hardness).

Initially the silicone base and silicone catalyst were merged before being combined with the CIP particles. Samples were produced by chaotic mixing of proportioned material components in a mixer at room temperature (22 °C). Degassing of the samples under adequate process vacuum followed. During decavitation, the shedding of iron particles results in the formation of ring structures as the cavities ascend and eventually dissipate.[17] Should the concentration be high enough to ensure contiguation of rings then capillary doublets occur.

For FTIR spectroscopy, it is essential that the samples be very thin to allow a high level of wave transmission, measurable using FTIR techniques. Using a simple press loaded with deadweights as shown in Figure 2, a constant compression force was applied to the uncured mixture for 1 h during crosslinking. Crosslinking

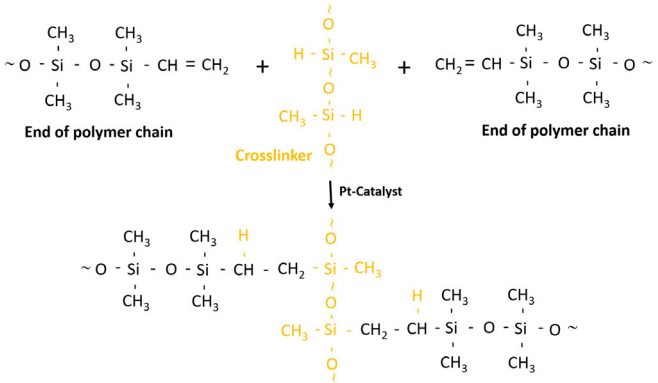

Figure 1. Crosslinking of silicone base and silicone catalyst.[15] [Color figure can be viewed at wileyonlinelibrary.com]

Table I. Crosslinking Time as a Function of Temperature SF00 (Silikonfabrik)

RTV-2 silicone SF00	
Temperature	Crosslinking time
< 10 °C	The crosslinking process is almost nonexistent
~ 23 °C	1.5 h[a]
~ 50 °C	Approximately 15 min[a]
~ 150 °C	Approximately 30 s[a]

[a] Depending on the thickness of the sample.

of the samples for Raman spectroscopy was completed after 4 h in a petri dish.

Aging tests on MAP have shown only degradation at high temperature over long periods and with high CIP concentrations as shown in Figure 3.[18]

Low CIP concentration MAP appears to be relatively free from aging, particularly at room temperature and therefore stability and reusability are rarely a problem.

EXPERIMENTAL APPARATUS

Samples with thicknesses of 0.1, 0.15, 0.2, and 0.25 mm and having CIP content of between 0 and 35 wt% were tested using a sample holder with a 23 mm diameter window, to which both axial and transverse magnetic fields were applied. Magnetic fields were generated using Nickel-plated sintered N42 NdFeB permanent magnets.[19]

For the axial polarized field, a simple 40 mm diameter (with 23 mm aperture) ring magnet as illustrated in Figure 4(a) was secured to the sample holder. The magnetic flux density varied from 30 mT at the center of the ring magnet to 80 mT at the inner edge of the ring magnet (outer sample window).

For the transverse field, two symmetrical 5 mm cube magnets were placed on the same fixture with the pole surfaces 25 mm apart (23 mm aperture diameter plus fixture wall thickness). The magnetic circuit was closed with a 2 mm thick iron ring as depicted in Figure 4(b). The magnetic flux density varied from 5 mT at the center between the magnets to 140 mT at the surface of the magnets (outer sample window).

FOURIER TRANSFORM INFRA-RED (FTIR) SPECTROSCOPY

In transmission spectroscopy methods such as FTIR, the infrared beam passes through the sample and the effective path length is determined by both the thickness of the sample and its orientation to the directional plane of the IR beam.[20]

Figure 5 shows the FTIR spectrum of PDMS [21] without CIP from which no appreciable difference between samples containing 35 wt% CIP (Figure 6) and those sans CIP can be observed. The same is true for samples containing 7, 12, 17, and 23 wt%. This is in line with other findings concerning FTIR spectra of polyurethane-based magnetorheological polymers with considerably higher CIP content, which reveal a mere shift in transmission amplitude through the material.[2]

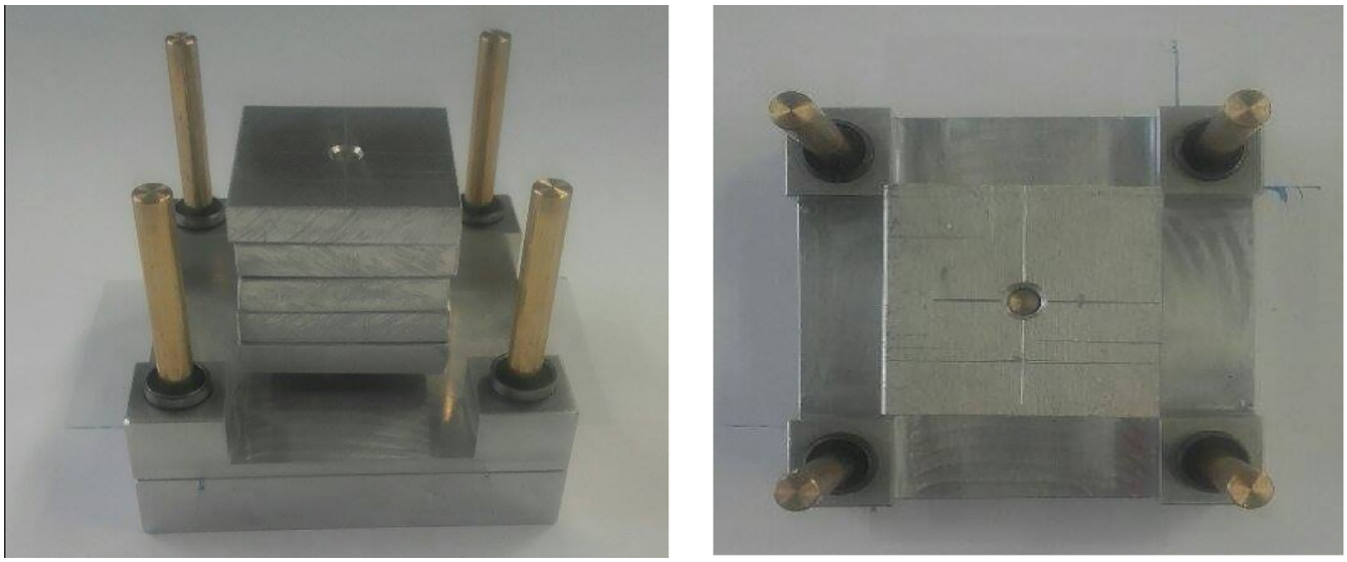

Figure 2. Simple press (10 × 10 cm) loaded with deadweights. [Color figure can be viewed at wileyonlinelibrary.com]

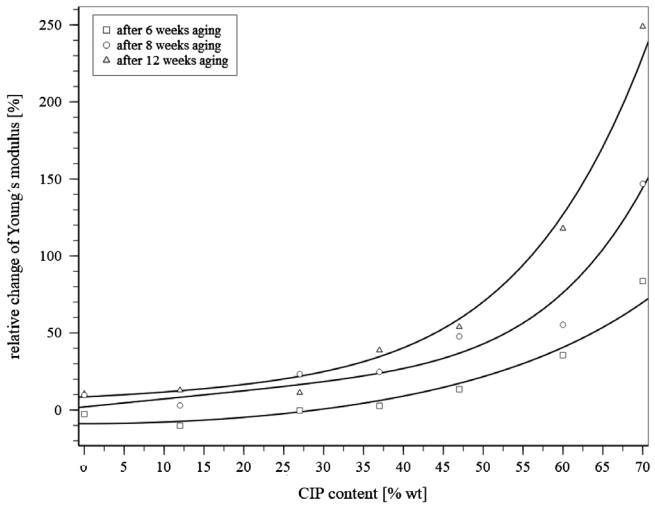

Figure 3. Effects of aging on MAP at elevated temperatures. [Color figure can be viewed at wileyonlinelibrary.com]

The only difference between Figure 5 and the following FTIR spectra are the average transmission values. While the average transmission values of PDMS samples without CIP are considerably higher, these correspondingly decrease with increasing CIP content.

For higher CIP concentrations, there is little difference except for changes in the average transmission level. Figure 6 shows an example for 35% CIP by weight. For the other samples containing 7, 12, 17, and 23 wt%, respectively, the curves follow an identical pattern.

Figure 7 reveals a slight, but noticeable, difference at a wavelength of 4.255 μm (wavenumber 2350 cm^{-1}) when the sample is subjected to a axial magnetic field. The black curve is the initial condition without magnetic field (oM1). The red curve denotes the condition following the application of a magnetic field (mM2) and blue represents the relaxation of the MAP immediately following removal of the magnetic field (oM3). However, this difference occurs exclusively for samples containing 2 wt% CIP.

The experiments were repeated for the same samples but under the influence of a transverse magnetic field. As shown in Figure 8, a similar effect can be seen at the same wavelength. In this case, the effect commences with samples containing more than 1.5 wt% CIP and reaches a maximum at 2 wt% CIP.

Again, the black curve is the initial condition without magnetic field (oM1). The red curve represents the situation following the application of a magnetic field (mM2) and blue depicts the relaxation of the MAP immediately following removal of the magnetic field (oM3). The relaxation continued over several hours before the MAP finally recovered its original condition as demonstrated by the black curves in Figures 7 and 8.

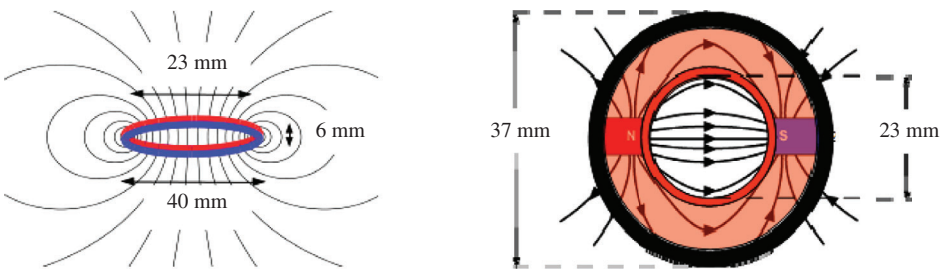

Figure 4. NdFeB magnets. (a) axial field; (b) transverse field. [Color figure can be viewed at wileyonlinelibrary.com]

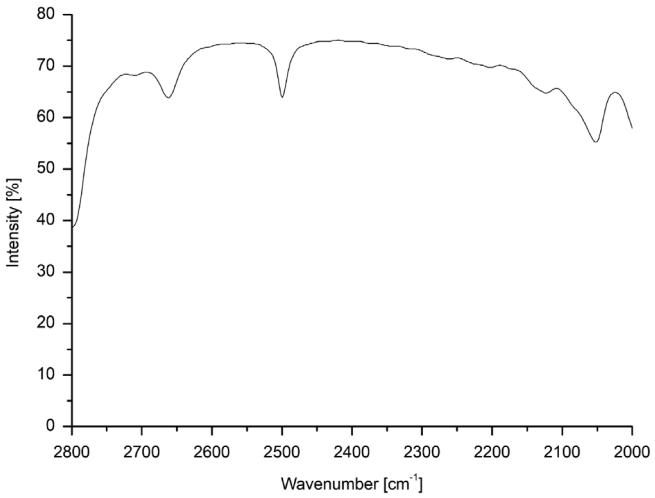

Figure 5. FTIR spectrum, PDMS alone. [Color figure can be viewed at wileyonlinelibrary.com]

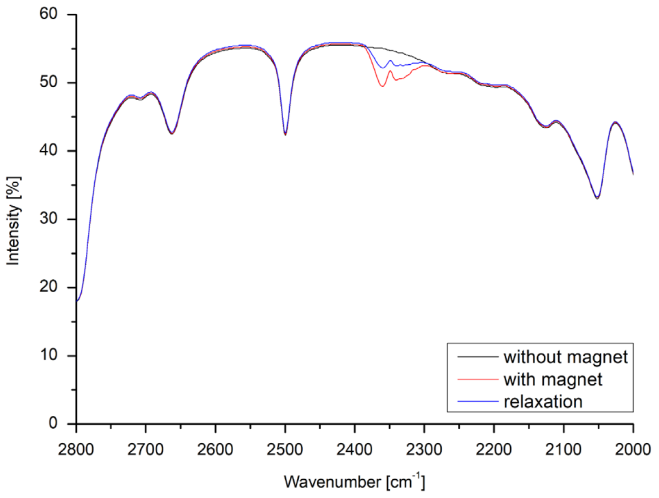

Figure 7. FTIR spectrum, MAP with 2 wt% of CIP in axial magnetic field. [Color figure can be viewed at wileyonlinelibrary.com]

The difference between IR transmission in the 2 wt% CIP samples, with and without magnetic field, is shown more clearly in the expanded graph of Figure 9 for PDMS with 2 wt% carbonyl iron powder.

The changes shown in Figures 7 and 8 (expanded in Figure 9) are not considerable but certainly observable and repeatable throughout a range of similar samples. Why this effect is only so clearly visible with 2 wt% CIP, will be explained later.

These experiments were repeated several times using the same and other, samples containing 2 wt% CIP. As illustrated in Figures 7 and 8, clear differences in the characteristic curves are observable only at a wavelength of 4.255 μm. Everywhere else in the spectrum there are only changes in average transmission level due to general opacity. It is interesting to observe that the effects start to become apparent with 1.5 wt% only under the influence of the transverse magnetic field, as shown in Figure 10, whereas for the axial magnetic field the effect remains absent until the 2 wt% level is reached.

However, samples containing 1 and 3 wt% CIP are largely unaffected by the influence of either a radial or a transverse magnetic field and merely resemble those for higher CIP concentrations, as can be seen from Figure 11.

Clearly, the IR absorption in MAP samples having 2 wt% CIP content shows the greatest magnetic field dependency, while those with 1.5 wt% exhibit changes only in a transverse magnetic field. Samples containing 1, 2.5, and 3 wt% reveal no measurable influence.

Raman Spectroscopy

Raman spectroscopy is used to observe vibrational, rotational and other low frequency modes in a system. It is often utilized as a supplement to infrared spectroscopy in chemistry to provide a fingerprint by which molecules can be identified. It relies on inelastic (Raman) scattering of monochromatic light. Coherent light usually results from a laser in the visible, near infrared, or

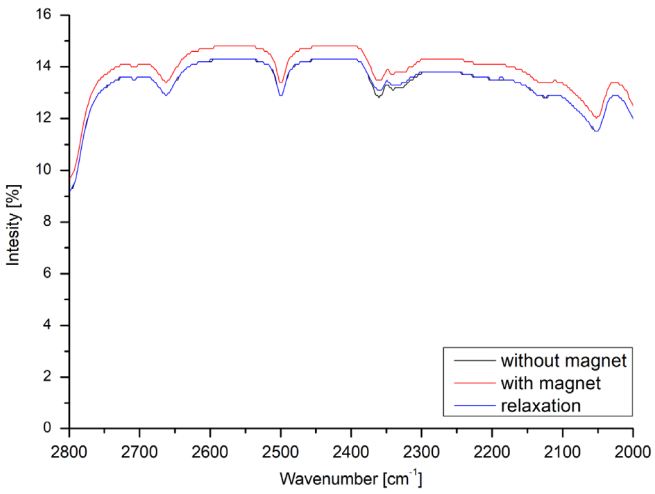

Figure 6. FTIR spectrum, MAP with 35 wt% of CIP. [Color figure can be viewed at wileyonlinelibrary.com]

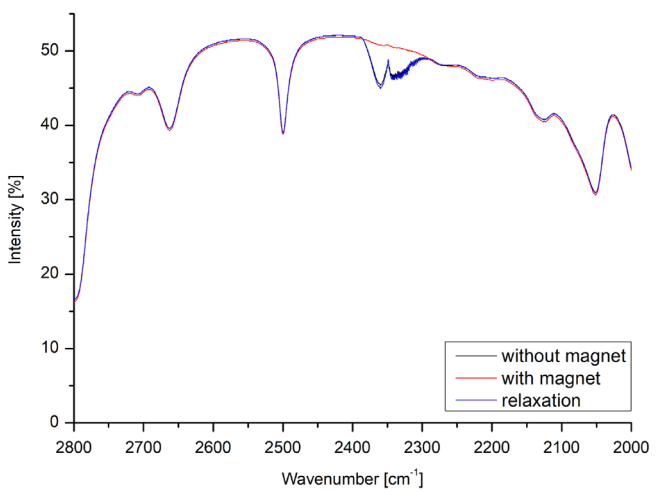

Figure 8. FTIR spectrum, MAP with 2 wt% of CIP, in transverse magnetic field. [Color figure can be viewed at wileyonlinelibrary.com]

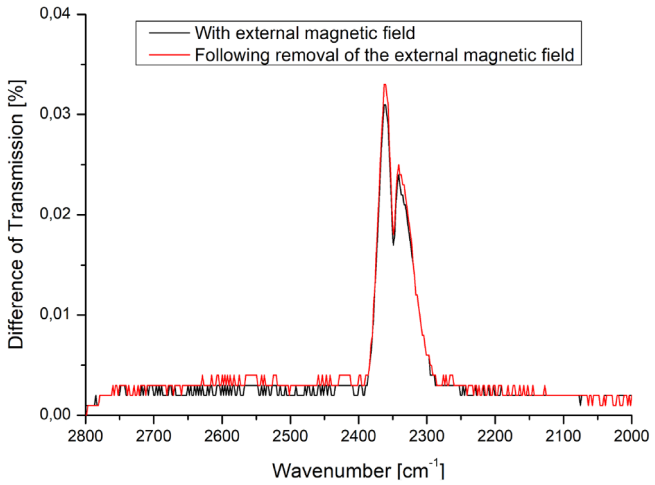

Figure 9. Transmission difference following application and removal of magnetic field. [Color figure can be viewed at wileyonlinelibrary.com]

near ultraviolet range. In this work, a laser with a wavelength of 798 nm (near infrared) was used. The laser light interacts with molecular vibrations, photons or other excitation in the system. Photon energy is shifted up or down according to the energy of the laser which in turn provides information concerning the vibrational modes in a system. Elastic scattered radiation at the wavelength corresponding to the laser line (Rayleigh scattering) is filtered out, while the remaining radiation is dispersed onto a detector.[22]

All the samples were tested using Raman spectroscopy. In principle, infrared spectroscopy and Raman spectroscopy complement each other in their information content.[23] Figure 12 illustrates the characteristic peaks of PDMS. These do not change with an increased proportion of CIP.

In contrast to FTIR, it is not possible to measure transmission spectra or detect relaxation processes with the help of Raman spectroscopy at all. These results indicate that relaxation phenomena are determined exclusively by internal conditions within the MAP. No phenomena could be detected on the surface.

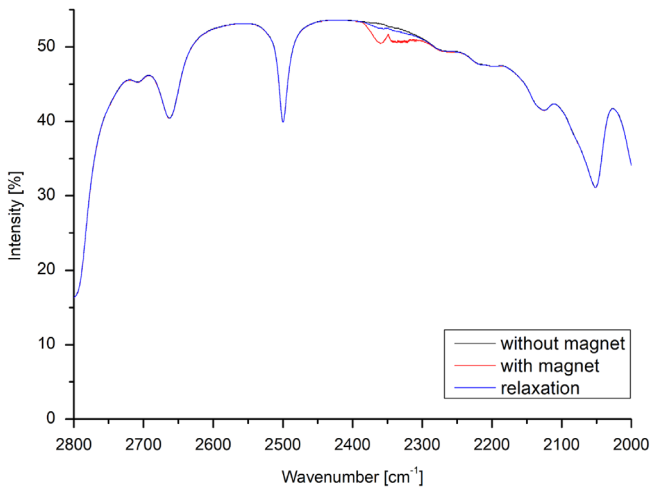

Figure 10. FTIR spectrum, MAP with 1.5 wt% of CIP in transverse magnetic field. [Color figure can be viewed at wileyonlinelibrary.com]

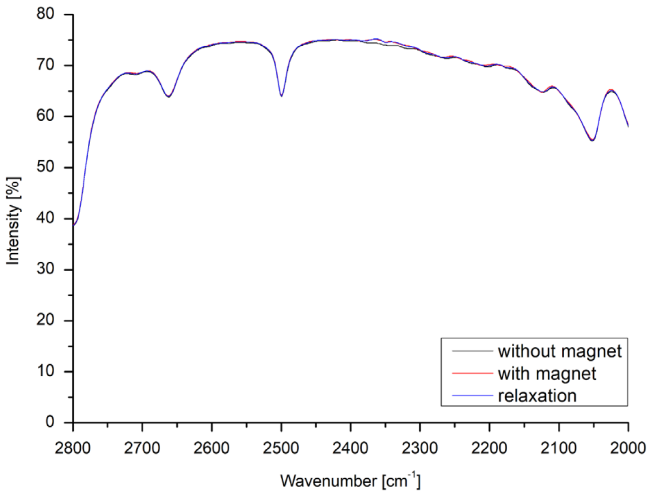

Figure 11. FTIR spectrum, MAP with 1.0 wt% CIP in axial magnetic field. [Color figure can be viewed at wileyonlinelibrary.com]

Observations

Conventional MAPs, containing higher CIP concentrations, exhibit little or no magnetically induced change over the entire IR electromagnetic spectrum. Only with very low CIP concentration, and particularly around 2 wt%, a magnetic influence can be observed and then only at a wavelength of 4.255 µm.

The band 2300 to 2400 cm^{-1} is indicative of carbon dioxide absorption and this effect disappears when the same measurements are made in a pure dry nitrogen atmosphere. However, the amount of CO_2 in air is merely 0.04% volume. CO_2 is diamagnetic with a molar magnetic susceptibility of $-20.88 \cdot 10^{-6}$ cm^3/mol[24] the modulus of which is greater than that of copper $-6.4 \cdot 10^{-6}$ cm^3/mol.[25] Nitrogen is also diamagnetic but has a magnetic susceptibility of only $-12 \cdot 10^{-6}$ cm^3/mol[25] and oxygen is paramagnetic with a magnetic susceptibility of $3335 \cdot 10^{-6}$ cm^3/mol.[24] Consequently, it is highly likely that the diamagnetic effects of CO_2 are responsible for the change in spectral absorption at this wavelength. Further experiments with 2 wt% MAP

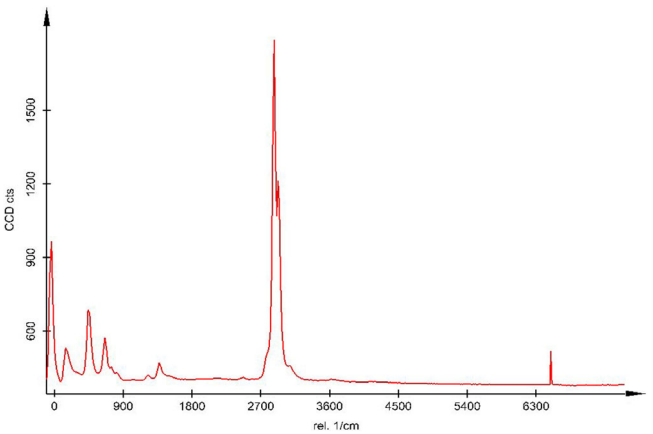

Figure 12. Raman spectrum, PDMS with and without CIP. [Color figure can be viewed at wileyonlinelibrary.com]

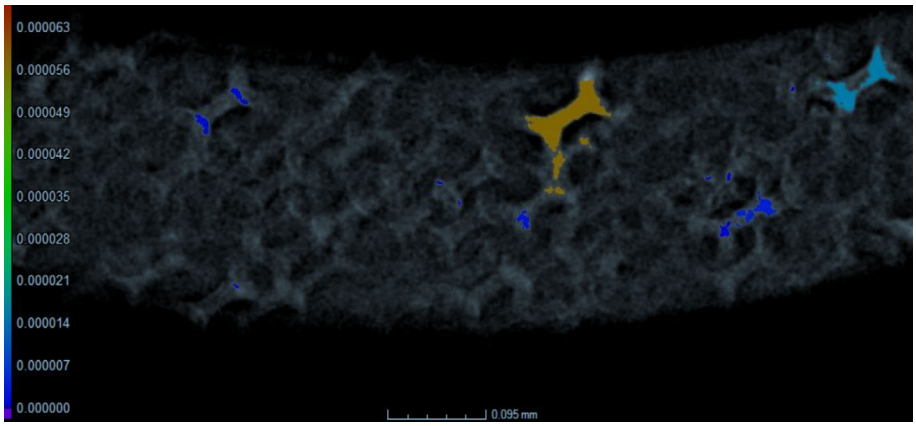

Figure 13. X-Ray CT of MAP with 2 wt% CIP. [Color figure can be viewed at wileyonlinelibrary.com]

containing other diamagnetic materials such as copper instead of CIP revealed no such magnetic field induced change in the IR spectra. Consequently, it can be concluded that the effect results from the interaction between 2 wt% CIP magnetoactive elastomer and diamagnetic CO_2.

The question arises as to why only samples containing 2 wt% CIP reveal any such effects. To ascertain the difference between 2 wt% and other CIP content MAP X-Ray tomography was employed. This reveals some very interesting internal structural formations, which appear only to exist at very low CIP concentrations.

X-Ray Analysis

MAP have previously been the subject of investigation using X-Ray diffraction techniques on magnetite-filled MAP.[26] In this work, the use of X-Ray radiation is restricted to 2D and 3D tomography for internal structure analysis purposes rather than spectroscopy. In this study, numerous samples with CIP content from 0 to 7 wt% were investigated using a GE Phönix v|tome|xs 240/180 X-Ray tomograph at 55 keV. Subsequent image analysis revealed some interesting structures with the MAP.

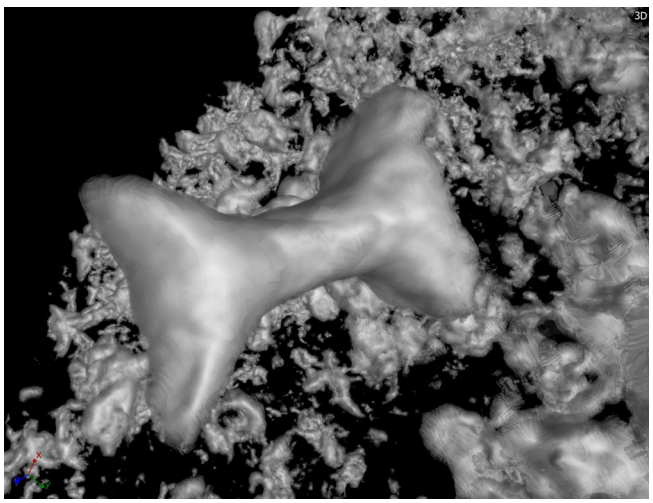

Figure 14. Single capillary doublet with slightly concave ends. [Color figure can be viewed at wileyonlinelibrary.com]

Prior to complete curing of the polymer, CIP collection around the periphery of ascending cavities results in ring formation as the 1 wt% CIP level is approached. At 1.5 wt% CIP content, the ring formation becomes complete and at 2 wt% bubble contiguation forces CIP into voids between the cavities resulting in the formation of capillary doublets. At higher CIP concentrations such ring formations tend to diminish and a more random anisotropic condition prevails.[17]

The 2 wt% CIP MAP samples are the only ones, which show appreciable change at any IR wavelength and particularly at 4.255 μm (wavenumber 2350 cm^{-1}). For these samples alone, an extremely clear structure becomes visible under X-ray computer tomography as can be seen in Figure 13.

Recourse to Figure 14 reveals the topology of the capillary bridges as often being only slightly concave.[27] This leads to a slight increase in the volume of the capillary doublet tending toward the critical 2 wt% level. At higher CIP concentrations, the CIP density exceeds the level at which such structures can form resulting in an almost amorphous topology as found in MAP with higher CIP concentration.[17]

CONCLUSIONS

For the first time, extensive spectral investigations concerning MAP with low CIP concentrations have been carried out. X-Ray tomography has revealed how, with relatively low concentrations of CIP, the formation of cavities in MAP cause the development of ring structures during gas evacuation. With increasing CIP concentration inter cavity capillary doublets are formed, which result in clearly measurable magnetic field dependent changes in IR absorption at a wavelength of 4.255 μm. This is almost certainly due to interactions between diamagnetic atmospheric CO_2 and the capillary doublet structures formed exclusively in MAP with CIP mass fraction between 1.5 and 3 wt%. Although the full effects (also on other diamagnetic gases) remain to be investigated, this inevitably has potential implications for future sensor devices.

ACKNOWLEDGMENTS

The authors would like to express their thanks to the German Research Federation (DFG) for financial support within the

SPP1681 (Grant MO 2196/2-1) research program and for the micro-computertomograph (Grant INST 102/11-1 FUGG). A special word of thanks to Birgit Striegl for the X-Ray analysis and Manfred Röhrl for assistance with the Raman and FTIR spectroscopy.

REFERENCES

1. Li, W. H.; Zhou, Y.; Tian, T. F. *Rheol Acta*. **2010**, *49*, 733. https://doi.org/10.1007/s00397-010-0446-9.
2. Xu, Y.; Gong, X.; Xuan, S.; Zhang, W.; Fan, Y. *Soft Matter*. **2011**, *7*, 5246. https://doi.org/10.1039/c1sm05301a.
3. Cleiton, J.; dos Santos, S.; Barbosa, O.; Ortiz, C.; Berenguer-Murcia, A.; Rodrigues, R. C.; Fernandez-Lafuente, R. *ChemCatChe*. **2015**, *7*, 2413. https://doi.org/10.1002/cctc.201500310.
4. Mayer, M.; Rabindranath, R.; Börner, J.; Hörner, E.; Bentz, A.; Salgado, J.; Han, H.; Böse, H.; Probst, J.; Shamonin, M.; Monkman, G. J.; Schlunck, G. *PLoS One*. **2013**, *8*(10), e76196. https://doi.org/10.1371/journal.pone.0076196.
5. Balasoiu, M.; Bica, I. *Res. Phys.* **2016**, *6*, 199.
6. Kuznetsova, I. E.; Kolesov, V. V.; Zaitsev, B. D.; Fionov, A. S.; Shihabudinov, A. M.; Stepanov, G. V.; Kramarenko, E. Y. *Bull. Russ. Acad. Sci. Phys.* **2017**, *8*, 945. https://doi.org/10.3103/S1062873817080184.
7. Forster, E.; Mayer, M.; Rabindranath, R.; Böse, H.; Schlunck, G.; Monkman, G. J.; Shamonin, M. *J. Appl. Polym. Sci.* **2013**, *128*(4), 2508. https://doi.org/10.1002/app.38500.
8. Nadasi, H., May K., Eremin A., & Stannarius R. Magnetoresponsive dispersions of anisometric pigment particles and gels, DFG SPP1681 Tagung, Benediktbeuern, **2016**.
9. Schatte, S., Seliger, J., Prevost S. & Gradzielski M. Magnetic nanocubes in worm-like micellar gels - *DFG SPP1681 Tagung*, Benediktbeuern **2016**.
10. Fuchs, A.; Sutrisno, J.; Gordaninejad, F.; Caglar, M. B.; Yanming, L. *J. Appl. Polym. Sci.* **2010**, *117*(2), 934. https://doi.org/10.1002/app.31533.
11. Garcia-Márquez, A.; Demortière, A.; Heinrich, B.; Guillon, D.; Bégin-Colin, S.; Donnio, B. *J. Mater. Chem.* **2011**, *21*(25), 8994. https://doi.org/10.1039/c1jm11381j.
12. Wei, B.; Gong, X.; Jiang, W. Influence of Polyurethane Properties on Mechanical Performances of Magnetorheological Elastomers; Wiley InterScience, **2009**, *116*, 771.
13. Kuo, A. C. M. Poly(dimethylsiloxane). In Polymer Data Handbook, Oxford University Press: University of Oxford, **1999**.
14. Hamciuc, C.; Hamciuc, E.; Okrasa, L. *Macromol. Res.* **2011**, *19*(3), 250. https://doi.org/10.1007/s13233-011-0311-4.
15. Wacker GmbH. (**2009**). PROCESSING RT V-2 SILICONE RUBBERS. Hg. v. Wacker GmbH. Wacker Chemie, München, checked on 2/13/2017.
16. Nguyen, N.-V.; Wu, J.-S.; Jen, C.-P. *BioChip J.* **2018**, *12*(4), 317. https://doi.org/10.1007/s13206-018-2402-1.
17. Sindersberger, D.; Prem, N.; Monkman, G. J. *J. Appl. Sci.* **2019**, *5*, 48291. https://doi.org/10.1002/app.48291.
18. Kerscher, S. T. Bachelor Thesis, Ostbayerische Technische Hochschule Regensburg, **2017**.
19. Supermagnete - Katalog, Webcraft GmbH https://www.supermagnete.de/ (Accessed May 28, 2018).
20. Griffiths, P.; De Haseth, J. A. Fourier Transform Infrared Spectrometry; *Wiley-Interscience*: Hoboken, NJ, **2007**.
21. Lambert, J.; Biele, C.; Marsmann, H. C. Strukturaufklärung in der organischen Chemie; Pearson: München, Germany, **2012**.
22. Baer, D. R.; Thevuthasan, S. Characterization of Thin Films and Coatings. In Handbook of Deposition Technologies for Films and Coatings, 3rd ed.; Elsevier: Amsterdam, Bosten, **2010**.
23. Banwell, C. N.; Mc Cash, E. M. Fundamentals of Molecular Spectroscopy; *McGraw-Hill Publishing Co*: London, UK, **1994**.
24. Havens, G. G. *Phys. Rev.* **1933**, *43*, 992. https://doi.org/10.1103/PhysRev.43.992.
25. Martienssen, W. Numerical Data and Functional Relationships in Science and Technology; Springer: Heidelberg, Germany, **1986**.
26. Petcharoen, K.; Sirivat, A. *Mater. Sci. Eng.* **2016**, *C61*, 312.
27. Gabrieli, F.; Lambert, P.; Cola, S.; Calvetti, F. *Int. J. Numer. Anal. Meth. Geomech.* **2011**, *36*, 918. https://doi.org/10.1002/nag.1038.